

# Reflective liquid-crystal displays with asymmetric incident and exit angles

Zhibing Ge and Thomas X. Wu

*Department of Electrical Engineering, University of Central Florida, Orlando, Florida 32816*

Xinyu Zhu and Shin-Tson Wu

*College of Optics and Photonics, University of Central Florida, Orlando, Florida 32816*

Received August 20, 2004; revised manuscript received October 13, 2004; accepted November 8, 2004

The  $2 \times 2$  matrix methods are extended to calculate the optical behaviors of reflective liquid-crystal displays with asymmetric incident and exit angles. Both the unfolding method and the backward-eigenwave method are employed to derive the  $2 \times 2$  matrix representations. The simulation results for symmetric incident and exit angles from these two methods are identical and agree well with those obtained from the  $4 \times 4$  matrix method when the air-panel surface reflections are neglected. Further, the derived  $2 \times 2$  matrix methods are applied to the asymmetric cases with different incident and exit angles. The simulated results on the normally black vertical alignment and normally white mixed-mode twisted nematic reflective displays show reasonably good agreement with the reported experimental data. In addition, a rubbing effect related to contrast values is observed and analyzed in asymmetric reflective cases. We also find that this effect has a significant influence on the contrast ratios once the difference between the incident and exit angles becomes large. © 2005 Optical Society of America

OCIS codes: 230.3720, 230.2090.

## 1. INTRODUCTION

Reflective liquid-crystal displays (LCDs) exhibit some unique advantages over transmissive ones in low power consumption, sunlight readability, and large aperture ratio, which lead to filmlike image quality.<sup>1</sup> They have been widely used in both direct-view and projection displays, such as personal digital assistants, cellular phones, and liquid-crystal-on-silicon-based projectors. With a reflective direct-view LCD, which uses ambient light to read out the displayed images, surface reflection becomes a critical issue. To minimize surface specular reflection for the purpose of enhancing contrast ratio, the ambient light is incident to the panel at an angle of approximately  $-30^\circ$ , and the displayed image is reflected by the embedded bumpy reflector to the observer at  $\sim 10^\circ$  off the normal direction, as shown in Fig. 1. That is, in a direct-view reflective LCD the incident and exit angles are not symmetric. Owing to the asymmetry of the input and output angles, the incident and reflected beams experience different LC director orientations. Most previous analyses that deal with reflective LCDs assume normal incidence. This assumption is valid only for projection displays but is invalid for direct-view reflective LCDs. Therefore a realistic analysis for reflective LCDs should consider this asymmetric feature.

In this paper we introduce two methods, the unfolding method and the backward-eigenwave method, for use in deriving the  $2 \times 2$  matrix representations for reflective LCDs with asymmetric incident and exit beams. In these methods, in order to account for the slant reflector, we derive a transformation matrix to correlate the exit and incident electric fields on the transition slant surface of the

reflector. Further, a reflectance defined on the basis of the energy-flow diagram is introduced to deal with the asymmetry on the panel surface. Finally, we apply our analyses to investigate two practical LC operation modes: normally black vertical alignment (VA)<sup>2</sup> and normally white mixed-mode twisted nematic (MTN)<sup>3</sup> cells. In simulations of reflective LCDs, the  $4 \times 4$  matrix method<sup>4-12</sup> is a commonly employed approach for calculating the optical performance under the conditions of symmetric incident and exit angles. However, to our best knowledge, no systematic studies of  $4 \times 4$  matrix method formulations under asymmetric incident and exit angles have ever been reported. Therefore to verify the accuracy of the  $2 \times 2$  methods here, we compare them with the well-known  $4 \times 4$  matrix method only under conditions in which the incident angle and the exit angle are equal. These results agree well once the surface reflection is eliminated by surface air coatings. However, in most practical direct-view reflective LCDs, the exit angle is intentionally deviated from the incident angle in order to avoid specular reflections. Thus our  $2 \times 2$  methods here provide a unique capability for simulating the realistic reflective LCD.

## 2. THEORETICAL ANALYSES

We consider that an unpolarized light enters an LC panel at an oblique angle and is reflected back to the air as shown in Fig. 2. Without loss of generality, we choose a coordinate system in which the wave vector  $k$  lies in the  $x-z$  plane. Here the  $+z$  axis points from the bottom glass substrate to the exit polarizer. The whole LCD system is

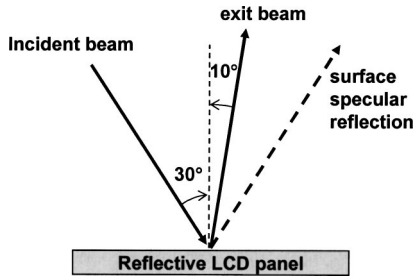


Fig. 1. Schematic diagram of beam path and viewing position in a conventional hand-held reflective LCD device.

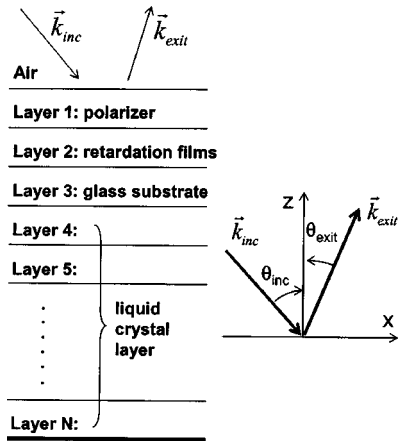


Fig. 2. Schematic diagram of layer division in a direct-view reflective LCD system. The wave-propagation vector  $k$  lies on the  $x-z$  plane,  $\theta_{inc}$  is the incident angle from the air to the LCD, and  $\theta_{exit}$  is the exit angle from the LCD to the air.

divided into  $N$  layers in the  $z$  direction. The retardation film shown in the figure can comprise more than one layer as needed. In simulations, each film is treated as a single homogenous layer. And in some reflective LCD devices, special antireflection (AR) coatings are deposited outside the polarizer. Under such a condition, Layer 1 should be the AR coatings instead of the polarizer.

### A. Unfolding Method

Because of the different incident and exit angles, the input and outgoing beams encounter different LC director orientations during propagation. To facilitate the simulation in the same coordinate system, we can transform the reflective LC cell into an equivalent double-cell transmissive structure by putting the mirror-image<sup>13</sup> stacks of reflective LCD system below the original ones as shown in Fig. 3. We call this method the unfolding method. Such an unfolding treatment still keeps the same reflected wave-vector value  $\vec{k}_{exit}$  as before. However, the incident wave vector  $\vec{k}_{inc}$  is replaced by its image in the equivalent transmissive LCD system as shown in Fig. 3.

In order for the optical simulation in each layer to be carried out, the distribution of the optical axis in each layer needs to be well defined. Owing to the unfolding conversion, the LC director distribution in the image stacks needs to be adjusted accordingly. Figure 4 shows the relationship between the equivalent mirror-image director and the original one. Here  $\vec{n}_1$  is the original LC director at an azimuthal angle  $\phi$  and a tilt angle  $\theta$ , and  $\vec{n}_2$

represents the corresponding mirror image. Since a director denotes the preferred orientation direction of only the local-domain LC molecules,  $\vec{n}$  and  $-\vec{n}$  are equivalent to each other.<sup>14</sup> Therefore we can translate  $\vec{n}_2$  to the equivalent director  $\vec{n}_3$  above the  $x-y$  plane, which is just the opposite extent of  $\vec{n}_2$ , as shown in Fig. 4. Clearly, one can find that the tilt angle  $\theta'$  of  $\vec{n}_3$  is equal to that of  $\vec{n}_1$  (i.e.,  $\theta' = \theta$ ), while its azimuthal angle  $\phi'$  is deviated by  $\pi$  from that of  $\vec{n}_1$ ; i.e.,  $\phi' = \phi \pm \pi$ .

From this conversion, the bottom image stacks also have their directors defined in the  $x-y$  plane as the original ones. Besides, several matrices are needed here in order to correlate the electric-field components incident on the panel surface with the outgoing ones after modulation.

### 1. Transformation Matrices in the Top and Bottom Stacks

With the above-mentioned LC director distribution, we can derive the  $2 \times 2$  extended Jones matrices for the lower mirror-image layers and the original LC stacks sepa-

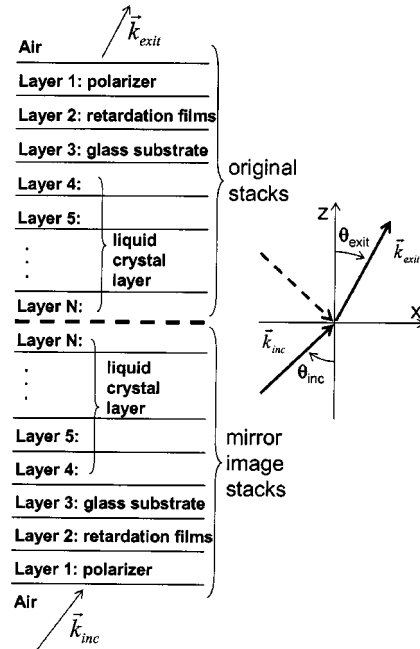


Fig. 3. Schematic diagram of layer division in an equivalent double-cell transmissive LCD structure by unfolding method. In this equivalent structure, light enters from the bottom air into the bottom polarizer layer and exits from the top polarizer layer to the top air.

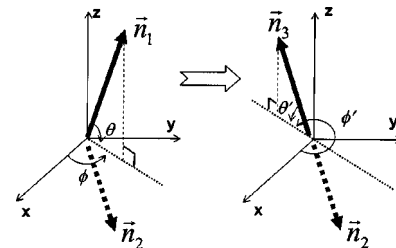


Fig. 4. Relationship between the image director and the original director in the same coordinate system.  $\vec{n}_1$ ,  $\vec{n}_2$ , and  $\vec{n}_3$  denote the original director, the mirror-image director, and the equivalent mirror-image director, respectively.

rately. Many efforts have been made to generalize the  $2 \times 2$  matrix formulations for birefringent media at oblique incidence.<sup>15–24</sup> Using the light-refraction principle, Yeh first discussed the case of a single birefringent plate by considering the boundary-matching conditions between isotropic and birefringent media.<sup>15</sup> Gu and Yeh later extended this method to multilayered systems, including LCDs. They assumed fictitious zero-thickness isotropic media between the birefringent plates.<sup>16</sup> On the other hand, Lien proposed another form of the extended Jones matrix, in which he accounted for the effects of Fresnel refraction at interfaces by matching only the electric-field boundary conditions.<sup>17</sup> Later, Lien and Chen introduced a modified  $2 \times 2$  matrix form, in which both the magnetic- and the electric-field boundary conditions are taken into consideration.<sup>18</sup> These  $2 \times 2$  matrix methods agree well with the  $4 \times 4$  matrix method for conventional twisted nematic transmissive cells.<sup>18</sup> Detailed comparisons among various  $2 \times 2$  matrix methods can be found in Ref. 20.

In our derivation of the  $2 \times 2$  matrix formulations of the case of asymmetric incidence and exit, we will follow the derivations of Lien's approach,<sup>17</sup> which has reasonably good accuracy. The overall extended Jones matrix representations of the upper original stacks ( $J_{\text{upper}}$ ) and lower mirror-image stacks ( $J_{\text{lower}}$ ) can be expressed as

$$J_{\text{upper}} = J_1 J_2 \dots J_{N-1} J_N, \quad (1)$$

$$J_{\text{lower}} = J'_N J'_{N-1} \dots J'_2 J'_1. \quad (2)$$

where  $J_i$  is the extended Jones matrix for the upper  $i$ th layer and  $J'_i$  corresponds to the  $i$ th mirror-image layer. Detailed derivations for  $J_i$  and  $J'_i$  formulations are described in Appendix A.

A special note regarding this unfolding treatment is that  $k_x$  should be adjusted to  $k_0 \sin \theta_{\text{exit}}$ , with  $k_0 = 2\pi/\lambda$  in calculating the element matrix  $J_i$  of the exit part  $J_{\text{upper}}$ , and to  $k_0 \sin \theta_{\text{inc}}$  for the  $J'_i$  of the incident part  $J_{\text{lower}}$ . Here  $\theta_{\text{inc}}$  is the incident angle from air to the display panel and  $\theta_{\text{exit}}$  represents the exit angle from the panel. In addition, the director tilt and azimuthal angles of the image stacks should be replaced by  $\theta'$  and  $\phi'$  as derived above, respectively.

Matrix  $J_{\text{lower}}$  in Eq. (2) acts as a transformation matrix that correlates the incident electric fields on the reflector-LC layer interface  $[E'_{x,N+1}, E'_{y,N+1}]^T$  with those on the air-panel interface  $[E'_{x,1}, E'_{y,1}]^T$ . Such a relationship can be expressed as

$$\begin{bmatrix} E'_{x,N+1} \\ E'_{y,N+1} \end{bmatrix} = J_{\text{lower}} \begin{bmatrix} E'_{x,1} \\ E'_{y,1} \end{bmatrix}. \quad (3)$$

Similarly,  $J_{\text{upper}}$  correlates the reflected electric fields on the air-panel interface  $[E'_{x,1}, E'_{y,1}]^T$  with those of the reflector-LC layer interface  $[E'_{x,N+1}, E'_{y,N+1}]^T$  as

$$\begin{bmatrix} E'_{x,1} \\ E'_{y,1} \end{bmatrix} = J_{\text{upper}} \begin{bmatrix} E'_{x,N+1} \\ E'_{y,N+1} \end{bmatrix}. \quad (4)$$

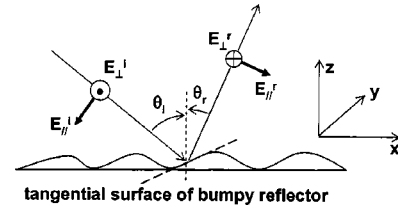


Fig. 5. Schematic diagram of the beam path in the LC cell and the field reflection on the surface of the reflector; the dashed line represents the tangential reflection surface on the bumpy reflector.

## 2. Transition Matrix on the Reflector Interference

In practical direct-view reflective LCDs, a slant bumpy reflector is intentionally designed to make the light exit angle different from the incident angle so that the images are deviated from the specular surface reflections. Owing to this special design, on the bumpy reflector surface the  $x$  and  $y$  components of the reflected electric field  $[E'_{x,N+1}, E'_{y,N+1}]^T$  are generally not equal to the corresponding incident fields  $[E^i_{x,N+1}, E^i_{y,N+1}]^T$ . However, they can be correlated by a transition matrix. Figure 5 depicts the field reflection diagram.

Figure 5 plots the electric-field orientations on the bumpy reflector surface. Here the light is incident at an angle  $\theta_i$  from the  $z$  axis and reflected at  $\theta_r$ . The tangential reflection surface on the reflector, shown as the dashed lines in Fig. 5, can always be uniquely defined. From Fig. 5 we can derive the following equations correlating the incident tangential-field components ( $x$  and  $y$  components) and their corresponding incident parallel ( $\parallel$ ) or perpendicular ( $\perp$ ) ones as

$$E'_{x,N+1} = -E^i_{\parallel,N+1} \cos \theta_i, \quad (5)$$

$$E'_{y,N+1} = -E^i_{\perp,N+1}. \quad (6)$$

Here  $E^i_{\parallel,N+1}$  and  $E^i_{\perp,N+1}$  are the parallel and perpendicular electric-field components impinging on the reflector surface, and their  $x$  and  $y$  components are  $E^i_{x,N+1}$  and  $E^i_{y,N+1}$ .  $\theta_i$  is the incident angle with respect to the  $+z$  axis and can be easily obtained by Snell's law as

$$\theta_i = \sin^{-1}(\sin \theta_{\text{inc}} n_{\text{LC}}). \quad (7)$$

Here  $n_{\text{LC}}$  stands for the average LC refractive index. From Fig. 5, similar relationships for the reflected electric fields can be expressed as

$$E^r_{x,N+1} = E^r_{\parallel,N+1} \cos \theta_r, \quad (8)$$

$$E^r_{y,N+1} = E^r_{\perp,N+1}, \quad (9)$$

$$\theta_r = \sin^{-1}(\sin \theta_{\text{exit}}/n_{\text{LC}}). \quad (10)$$

In a reflective LCD, aluminum is commonly used as the bumpy reflector. The metallic reflector can be assumed to be a perfect conductor; thus the reflected electric and incident fields have equal parallel and perpendicular amplitudes. This relation leads to

$$\begin{bmatrix} E_{x,N+1}^r \\ E_{y,N+1}^r \end{bmatrix} = \begin{bmatrix} -\frac{\cos \theta_r}{\cos \theta_i} & 0 \\ 0 & -1 \end{bmatrix} \begin{bmatrix} E_{x,N+1}^i \\ E_{y,N+1}^i \end{bmatrix}. \quad (11)$$

The minus signs in Eq. (11) denote one  $\pi$  phase change by the metallic reflector. Therefore the transition matrix  $J_{\text{TR}}$  can be written as

$$J_{\text{TR}} = \begin{bmatrix} -\frac{\cos \theta_r}{\cos \theta_i} & 0 \\ 0 & -1 \end{bmatrix}. \quad (12)$$

This matrix  $J_{\text{TR}}$  accounts for the slant shape of the reflector. With matrices  $J_{\text{TR}}$ ,  $J_{\text{lower}}$ , and  $J_{\text{upper}}$ , the  $x$  and  $y$  components of the electric fields between the exit and the incident waves just beneath the surface of LCD panel can be correlated as

$$\begin{bmatrix} E_{x,1}^r \\ E_{y,1}^r \end{bmatrix} = J_{\text{upper}} J_{\text{TR}} J_{\text{lower}} \begin{bmatrix} E_{x,1}^i \\ E_{y,1}^i \end{bmatrix}, \quad (13)$$

where

$$J_{\text{upper}} J_{\text{TR}} J_{\text{lower}} = J_1 J_2 \dots J_{N-1} J_N J_{\text{TR}} J_N' J_{N-1}' \dots J_2' J_1'. \quad (14)$$

### 3. Interface Matrices Induced from Index Mismatch

Considering the loss at the air–panel interface due to the refractive index mismatch, two additional interface matrices need to be introduced.<sup>17,21</sup> In the entrance side, the interface matrix is

$$J_{\text{ent}} = \begin{bmatrix} \frac{2 \cos \theta_1'}{\cos \theta_1' + n_1 \cos \theta_{\text{inc}}} & 0 \\ 0 & \frac{2 \cos \theta_{\text{inc}}}{\cos \theta_{\text{inc}} + n_1 \cos \theta_1'} \end{bmatrix}, \quad (15)$$

where  $\theta_1'$  is the light incident angle in the first layer under the panel surface and can be obtained by Snell's law as  $\theta_1' = \sin^{-1}(\sin \theta_{\text{inc}}/n_1)$ , while  $n_1$  stands for the average value of the real parts of  $n_e$  and  $n_o$  of the first layer under the surface, such as the first layer of the AR coatings or the polarizer. On the exit side, the interface matrix becomes

$$J_{\text{ext}} = \begin{bmatrix} \frac{2n_1 \cos \theta_{\text{exit}}}{\cos \theta_1 + n_1 \cos \theta_{\text{exit}}} & 0 \\ 0 & \frac{2n_1 \cos \theta_1}{\cos \theta_{\text{exit}} + n_1 \cos \theta_1} \end{bmatrix}, \quad (16)$$

and similarly  $\theta_1 = \sin^{-1}(\sin \theta_{\text{exit}}/n_1)$ .

Therefore the overall  $2 \times 2$  matrix representation for the whole system can be written as follows:

$$J = J_{\text{ext}} J_1 J_2 \dots J_{N-1} J_N J_{\text{TR}} J_N' J_{N-1}' \dots J_2' J_1' J_{\text{ent}}. \quad (17)$$

With this  $2 \times 2$  matrix  $J$ , the exit tangential electric fields becomes

$$\begin{bmatrix} E_{x,\text{air}}^{\text{exit}} \\ E_{y,\text{air}}^{\text{exit}} \end{bmatrix} = J \begin{bmatrix} E_{x,\text{air}}^{\text{inc}} \\ E_{y,\text{air}}^{\text{inc}} \end{bmatrix}, \quad (18)$$

where  $[E_{x,\text{air}}^{\text{inc}}, E_{y,\text{air}}^{\text{inc}}]^T$  and  $[E_{x,\text{air}}^{\text{exit}}, E_{y,\text{air}}^{\text{exit}}]^T$  denote the incident and the exit tangential electric fields, respectively, in air.

### 4. Reflectance Correction Coefficient Based on Energy-Flow diagram

In common reflective LCD systems, the incident light is usually from a diffusive light source, such as ceiling light or sunlight, rather than from a point source. However, in a real display panel characterization, the LCD panel is usually illuminated by a highly collimated light. Thus the incident and exit lights can be assumed to uniformly enter or exit the LCD panel. In other words, the incident light is not focused and can be assumed to impinge on the panel surface in parallel. Therefore the power of the incident or the exit light can be expressed as the product of the intensity and its transverse area along the propagation direction. For symmetric incidence and exit, the transverse areas for the two lights are equal. In such a condition, the reflectance is defined as the ratio of the reflected (output) power to the incident (input) power in the following form:

$$R = \frac{P_{\text{out}}}{P_{\text{in}}} = \frac{|E_{x,\text{air}}^{\text{exit}}/\cos \theta_{\text{exit}}|^2 + |E_{y,\text{air}}^{\text{exit}}|^2}{|E_{x,\text{air}}^{\text{inc}}/\cos \theta_{\text{inc}}|^2 + |E_{y,\text{air}}^{\text{inc}}|^2}. \quad (19)$$

However, for the case of asymmetric incidence and exit, the incident and exit beams have different transverse areas along the propagation direction in the air. Therefore the ratio of the areas should be taken into consideration. Figure 6 shows a plot of the beam path for the incident and exit waves. The incident beam has a transverse length  $AD$ , and that of the exit beam is  $KL$ . Therefore, since the covered ranges for the two lights in the  $y$  direction are equal, the input power and the exit power in these cases can be defined as

$$P_{\text{in}} = (|E_{x,\text{air}}^{\text{inc}}/\cos \theta_{\text{inc}}|^2 + |E_{y,\text{air}}^{\text{inc}}|^2)AD, \quad (20)$$

and the output power to air is

$$P_{\text{out}} = (|E_{x,\text{air}}^{\text{exit}}/\cos \theta_{\text{exit}}|^2 + |E_{y,\text{air}}^{\text{exit}}|^2)KL. \quad (21)$$

The ratio of  $KL$  to  $AD$  can be obtained from the geometric relations as shown in Fig. 6. The values of the refractive indices of the LCD layers (e.g., polarizer, glass, and

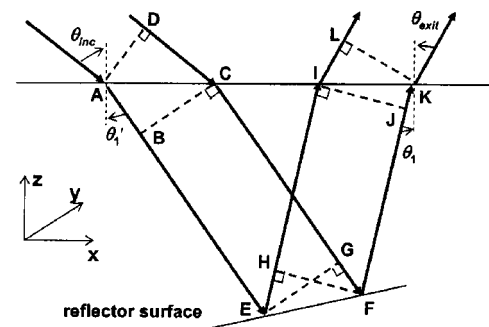


Fig. 6. Schematic diagram of energy-flow-defined reflectance with asymmetric incident and exit angles in  $R$ -mode LCD.

LC) are usually rather close; therefore the incident and exit beams experience negligible change in propagation direction in the LC panel. From the theory of geometry, triangles  $EFG$  and  $EFH$  are equivalent to each other. This results in  $EG=HF$ , which further leads to  $BC=IJ$ . Since  $BC=AC \cos \theta'_1$  and  $IJ=IK \cos \theta_1$ ,  $AC$  and  $IK$  will have the following relation:

$$AC \cos \theta'_1 = IK \cos \theta_1. \quad (22)$$

Moreover, since  $AD=AC \cos \theta_{\text{inc}}$  and  $KL=IK \cos \theta_{\text{exit}}$ , the ratio of  $KL$  to  $AD$  becomes

$$\eta_{\text{corr}} = \frac{KL}{AD} = \frac{IK \cos \theta_{\text{exit}}}{AC \cos \theta_{\text{inc}}} = \frac{\cos \theta'_1}{\cos \theta_1} \cdot \frac{\cos \theta_{\text{exit}}}{\cos \theta_{\text{inc}}}. \quad (23)$$

We define this ratio as  $\eta_{\text{corr}}$ , which is a correction coefficient of the reflectance for the asymmetric cases. It is easy to prove that  $\eta_{\text{corr}}$  is equal to 1 if the incident and exit angles are equal. Here if the average index difference between different layers is large, the shift of the beam path needs to be considered into the form of  $\eta_{\text{corr}}$ .

From Eqs. (20)–(23) the reflectance has the following expression:

$$R = \frac{P_{\text{out}}}{P_{\text{in}}} = \frac{|E_{x,\text{air}}^{\text{exit}}/\cos \theta_{\text{exit}}|^2 + |E_{y,\text{air}}^{\text{exit}}|^2 \cos \theta'_1}{|E_{x,\text{air}}^{\text{inc}}/\cos \theta_{\text{inc}}|^2 + |E_{y,\text{air}}^{\text{inc}}|^2 \cos \theta_1} \cdot \frac{\cos \theta_{\text{exit}}}{\cos \theta_{\text{inc}}}. \quad (24)$$

If we consider an unpolarized light with equal TE and TM components, we can assume

$$P_{\text{out}} = \left( \frac{|J_{11}|^2 \cos^2 \theta_{\text{inc}} + |J_{12}|^2 + J_{11} \cos \theta_{\text{inc}} J_{12}^* e^{-j\varphi} + J_{11}^* \cos \theta_{\text{inc}} J_{12} e^{j\varphi}}{\cos^2 \theta_{\text{exit}}} + |J_{21}|^2 \cos^2 \theta_{\text{inc}} + |J_{22}|^2 + J_{21} \cos \theta_{\text{inc}} J_{22}^* e^{-j\varphi} + J_{21}^* \cos \theta_{\text{inc}} J_{22} e^{j\varphi} \right) KL. \quad (31)$$

If we take the average value of  $P_{\text{out}}$  with respect to the phase  $\varphi$ , the average output power can be given as

$$P_{\text{out}}^{\text{av}} = \left( \frac{|J_{11}|^2 \cos^2 \theta_{\text{inc}} + |J_{12}|^2}{\cos^2 \theta_{\text{exit}}} + |J_{21}|^2 \cos^2 \theta_{\text{inc}} + |J_{22}|^2 \right) KL. \quad (32)$$

From Eqs. (26) and (32), the overall reflectance of an unpolarized light is given as

$$R = \frac{|J_{11}|^2 \cos^2 \theta_{\text{inc}} + |J_{12}|^2 + \cos^2 \theta_{\text{exit}} (|J_{21}|^2 \cos^2 \theta_{\text{inc}} + |J_{22}|^2)}{2 \cos^2 \theta_{\text{exit}}} \times \frac{\cos \theta'_1 \cos \theta_{\text{exit}}}{\cos \theta_1 \cos \theta_{\text{inc}}}. \quad (33)$$

## B. Backward-Eigenwave Method

In this section, another method to calculate the system  $2 \times 2$  matrix for reflective LCDs with asymmetric incident

$$\begin{bmatrix} E_{x,\text{air}}^{\text{inc}} \\ E_{y,\text{air}}^{\text{inc}} \end{bmatrix} = \begin{bmatrix} \cos \theta_{\text{inc}} \\ e^{j\varphi} \end{bmatrix}, \quad (25)$$

where  $\varphi$  denotes the phase difference between the TE and the TM components.

Equations (20) and (25) will result in

$$P_{\text{in}} = \left( \left| \frac{E_{x,\text{air}}^{\text{inc}}}{\cos \theta_{\text{inc}}} \right|^2 + |E_{x,\text{air}}^{\text{inc}}|^2 \right) AD = 2AD. \quad (26)$$

The  $x$  and  $y$  components of exit electric fields can be obtained from Eq. (18) as

$$\begin{bmatrix} E_{x,\text{air}}^{\text{exit}} \\ E_{y,\text{air}}^{\text{exit}} \end{bmatrix} = \begin{bmatrix} J_{11} & J_{12} \\ J_{21} & J_{22} \end{bmatrix} \begin{bmatrix} E_{x,\text{air}}^{\text{inc}} \\ E_{y,\text{air}}^{\text{inc}} \end{bmatrix}. \quad (27)$$

Expanding this equation, along with Eq. (25), leads to

$$E_{x,\text{air}}^{\text{exit}} = J_{11} \cos \theta_{\text{inc}} + J_{12} e^{j\varphi}, \quad (28)$$

$$E_{y,\text{air}}^{\text{exit}} = J_{21} \cos \theta_{\text{inc}} + J_{22} e^{j\varphi}. \quad (29)$$

Therefore the output power can be expressed as

$$P_{\text{out}} = \left( \left| \frac{E_{x,\text{air}}^{\text{exit}}}{\cos \theta_{\text{exit}}} \right|^2 + |E_{x,\text{air}}^{\text{exit}}|^2 \right) KL. \quad (30)$$

We can expand the  $P_{\text{out}}$ , and it will have the following form:

and exit angles is introduced. This method takes advantage of the eigenwaves' properties in a LC cell.

In an LC cell, if a forward wave propagates from bottom to top as shown by the bold arrows in Fig. 7, a backward wave (the dashed arrow lines) that stands for the reflected one will be excited simultaneously, and these two waves will have the same angles  $\theta$  with respect to the normal direction. With the symmetry relationship from reversal invariance of Maxwell's laws<sup>12</sup> in the LCD system, we can obtain simultaneously the  $2 \times 2$  element matrices to correlate the field components of both forward and backward waves between two subsequent homogeneous layers. In a reflective LCD with asymmetric incident and exit angles, the incident wave can be viewed as the corresponding backward part of a forward wave with an angle of  $\theta_{\text{inc}}$ , and the reflected wave can be taken as the forward wave with an angle of  $\theta_{\text{exit}}$ , as illustrated in Fig. 7. With this treatment, we can solve the wave-propagating problem in a LC system with an angle of  $\theta_{\text{inc}}$  to obtain the backward matrix. This matrix can further correlate the field components in the incident beam between two layers

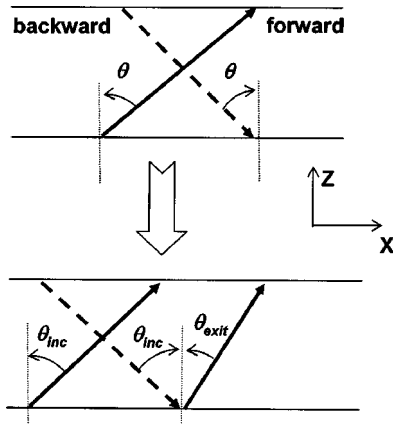


Fig. 7. The top figure shows schematically the forward propagation (bold arrow) and backward propagation (dashed arrow) through a layer. The bottom figure shows that the incident wave from top to bottom can be viewed as the backward part (dashed arrow) with an angle of  $\theta_{inc}$ .

in the asymmetric light incidence and exit. Similarly, we can solve that wave-propagating system but with an angle of  $\theta_{exit}$  to obtain the forward matrix, which can correlate the field components between two layers in the reflected beam in the above-mentioned asymmetric case. Therefore the two matrices can be derived in the same  $xyz$  coordinate. It does not require any special transformation of director distribution, unlike the image treatment in the unfolding method. We call this method the backward-eigenwave method.

Here, to obtain the formulations of the backward and forward  $2 \times 2$  matrices, we need to solve the eigenwaves of the  $4 \times 4$  coupling matrix as in the derivations of the conventional  $4 \times 4$  matrix method. The  $4 \times 4$  matrix method by solving eigenwaves was originally proposed by Eidner *et al.*<sup>9</sup> Stallinga<sup>12</sup> later further extended this scheme in deriving the  $4 \times 4$  matrix method to reflective LCDs. In Ref. 12, the computing speed is improved by a factor of 2 by use of the symmetry relation from the reversal invariance of Maxwell's laws. Here the faster speed by a factor of 2 could also be obtained by using the analytic approach with the Lagrange–Sylvester extrapolation polynomial.<sup>6,7,11</sup> In Appendix B we provide a systematic derivation of the  $4 \times 4$  matrix and its eigenwaves, which further generates the formulations of the  $2 \times 2$  element matrices for the backward-eigenwave method discussed later in this paper.

Returning to the reflective LCD structure as in Fig. 2, the incident tangential fields on the interface of the reflector–LC layer  $[E_{x,N+1}^i, E_{y,N+1}^i]^T$  and the fields on the air–panel interface  $[E_{x,1}^i, E_{y,1}^i]^T$  can be correlated once we define the overall transforming matrix in the inside stacks for the incident wave as  $J_e^{inc}$ . Their relation can be shown as

$$\begin{bmatrix} E_{x,N+1}^i \\ E_{y,N+1}^i \end{bmatrix} = J_e^{inc} \begin{bmatrix} E_{x,1}^i \\ E_{y,1}^i \end{bmatrix}, \quad (34)$$

with

$$J_e^{inc} = (J_{e,N}^-)^{-1} (J_{e,N-1}^-)^{-1} \dots (J_{e,2}^-)^{-1} (J_{e,1}^-)^{-1}, \quad (35)$$

where  $k_x = k_0 \sin \theta_{inc}$ . Similarly, we can define the overall transforming matrix in the inside stacks for the reflected

wave as  $J_e^r$ , which correlates the reflected electric fields on the air–panel interface  $[E_{x,1}^r, E_{y,1}^r]^T$  with those on the interface of the reflector–LC layer  $[E_{x,N+1}^r, E_{y,N+1}^r]^T$  as

$$\begin{bmatrix} E_{x,1}^r \\ E_{y,1}^r \end{bmatrix} = J_e^r \begin{bmatrix} E_{x,N+1}^r \\ E_{y,N+1}^r \end{bmatrix}, \quad (36)$$

with

$$J_e^r = J_{e,1}^+ J_{e,2}^+ \dots J_{e,N-1}^+ J_{e,N}^+, \quad (37)$$

where  $k_x = k_0 \sin \theta_{exit}$ . The detailed formulations for element matrices  $J_{e,i}^-$  of  $J_e^{inc}$  and  $J_{e,i}^+$  of  $J_e^r$  are provided in Appendix B.

With the transition matrix  $J_{TR}$  in Eq. (12) and surface compensation matrices  $J_{ext}$  and  $J_{ext}$ , we can express the overall  $2 \times 2$  matrix formulation for electric fields for the reflective LCDs as

$$J_e = J_{ext} J_e^r J_{TR} J_e^{inc} J_{ext}. \quad (38)$$

By inserting matrix  $J_e$  into Eq. (33), we can obtain the overall reflectance.

### 3. NUMERICAL EXAMPLES

To illustrate these  $2 \times 2$  matrix methods, we give some numerical examples for the two commonly employed reflective LC modes: normally black VA and normally white MTN cells.

For the VA mode, we chose MLC-6608 (from Merck) as the LC material. Its parameters are  $n_e = 1.5578$ ,  $n_o = 1.4748$ ,  $\epsilon_{||} = 3.6$ ,  $\epsilon_{\perp} = 7.8$ ,  $K_{11} = 16.7$  pN,  $K_{22} = 7.0$  pN, and  $K_{33} = 18.1$  pN. For the MTN mode simulations, we chose ZLI-4792 (from Merck). The material parameters are  $n_e = 1.5763$ ,  $n_o = 1.4794$ ,  $\epsilon_{||} = 8.3$ ,  $\epsilon_{\perp} = 3.1$ ,  $K_{11} = 13.2$  pN,  $K_{22} = 6.5$  pN, and  $K_{33} = 18.3$  pN.

A single polarizer with a broadband quarter-wave film is used to work as cross-polarizer structure for the direct-view reflective display. The complex polarizer refractive indices are assumed to have  $n_e = 1.5 + j0.00220820$  and  $n_o = 1.5 + j0.00003222$  with  $j = \sqrt{-1}$ , and the thickness of the polarizer is  $190 \mu\text{m}$ . For the broadband quarter-wave film, we use the structure shown in Fig. 8, which is composed of a chromatic quarter-wave film and a chromatic half-wave film.<sup>25</sup> The  $n_e$  of the quarter-wave film is 1.5110 and the  $n_o$  is 1.5095, with a film thickness of  $91.6667 \mu\text{m}$

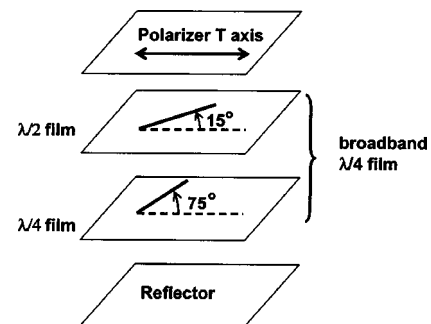


Fig. 8. Structure of a broadband quarter-wave film, which comprises one chromatic quarter-wave film and one chromatic half-wave film. The quarter-wave film has an optic axis with an angle of  $75^\circ$  to the transmission axis of the polarizer. The half-wave film has an angle of  $15^\circ$  to the transmission axis of the polarizer.

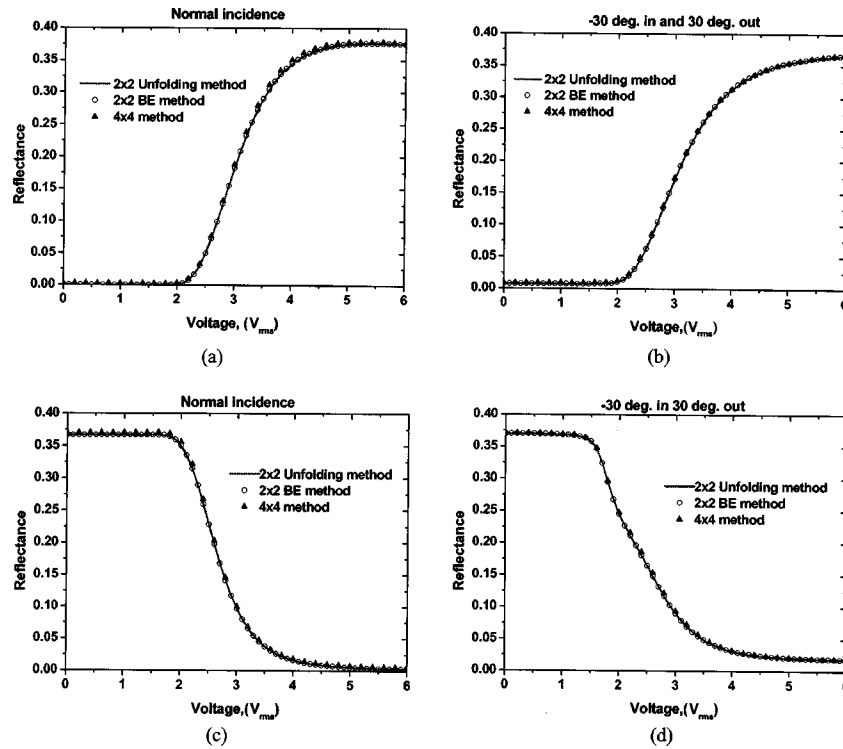


Fig. 9. Electro-optical properties of symmetric incidence for (a) normal incidence case with different methods for a VA mode, (b)  $\theta_{\text{inc}} = -30^\circ$  and  $\theta_{\text{exit}} = 30^\circ$  with different methods for a VA mode, (c) normal-incidence case with different methods for an  $80^\circ$  MTN mode, (d)  $\theta_{\text{inc}} = -30^\circ$  and  $\theta_{\text{exit}} = 30^\circ$  with different methods for an  $80^\circ$  MTN mode.

(at  $\lambda = 550$  nm). The half-wave film has  $n_o = 1.5123$  and  $n_e = 1.5089$  with a film thickness of  $80.8824 \mu\text{m}$  (at  $\lambda = 550$  nm).

For the case of symmetric incidence (including normal incidence), we employ the  $2 \times 2$  unfolding method and the  $2 \times 2$  backward-eigenwave method and compare results with those of the well-established  $4 \times 4$  matrix method. The  $4 \times 4$  matrix method takes in the specular panel surface reflections, which the  $2 \times 2$  matrix methods will not include. Therefore in this part of the simulation, the AR coating is introduced on the surface of the polarizer to eliminate the effect of symmetric specular surface reflections. Once validated, the  $2 \times 2$  matrix methods are extended to the asymmetric incident- and exit-angle case, in which, to our knowledge, no systematic  $4 \times 4$  matrix method formulations have ever been studied. In these cases, the surface reflection is greatly eliminated by the offset reflectance mechanism.<sup>26</sup> Therefore the AR coating is removed from our simulation. In all, our methods presented here enable us to optimize realistic reflective LCDs.

### A. Symmetric Incidence Case

The VA mode has been widely used in reflective LCDs owing to its high contrast ratio. The LC cell gap in our simulation is  $2.2 \mu\text{m}$  with a pretilt angle of  $88^\circ$ . Figures 9(a) and 9(b) show the simulated voltage-dependent reflectance curves from the unfolding backward-eigenwave and the  $4 \times 4$  matrix methods for the normal incidence and the symmetric oblique incidence ( $\theta_{\text{inc}} = -30^\circ$  and  $\theta_{\text{exit}} = 30^\circ$ ) cases, respectively. From these figures, the three methods agree very well. The results of the unfolding and the

backward-eigenwave methods are identical to each other. A negligible discrepancy between the  $2 \times 2$  and the  $4 \times 4$  matrix methods is found, which stems from the weak internal multiple reflections between different layers. Here the surface reflections have already been greatly eliminated by the panel's AR coating.

The MTN cell is also commonly used in reflective LCDs because of its large cell-gap tolerance and simple fabrication process. Figures 9(c) and 9(d) show the VR curves of a normally white  $80^\circ$  MTN mode from these three methods for normal incidence and symmetric oblique incidence ( $\theta_{\text{inc}} = -30^\circ$  and  $\theta_{\text{exit}} = 30^\circ$ ) cases, respectively. In the simulations, the LC cell gap is controlled at  $d = 2.81 \mu\text{m}$  and the pretilt angle is  $2^\circ$ . Similarly, excellent agreement between these methods are observed from these figures when the surface reflection is eliminated by the panel's AR coating.

### B. Asymmetric-Incidence Case

In the case of asymmetric incidence and exit, we will apply the derived  $2 \times 2$  matrix methods to calculate the optical performance of a real reflective LCD with slant microreflector. Among all the performance parameters, contrast ratio is the most critical figure of merit in direct-view reflective displays, as it is directly affected by the quality of the dark state. In direct-view reflective LCDs, two main factors determine the contrast ratios: surface reflection and light leakage in the dark state. Regarding the surface-reflection, in order to avoid overlapping the exit lights with specular reflections the ambient light usually illuminates the LCD panel at  $-30^\circ$  and the modulated light is guided out of the panel to the viewer in a

cone from  $0^\circ$  to  $+20^\circ$  with respect to the normal direction of the panel.<sup>26</sup> This type of distribution cone of light is caused by the nonideal surface roughness.<sup>26</sup> This treatment in practical reflective LCDs will greatly reduce the effect of specular surface reflection, and this reduction enhances the contrast ratio of the real device.

Besides the surface reflection, the light leakage from LC cell is also critical in determining the contrast ratio. Smaller residual phase retardation in the dark state will lead to a higher contrast ratio. The overall phase retardation is a summation of those accumulated values from both incident and exit beams. However, when the incident and exit angles are different in the fixed study coordinate, the rubbing diagram of boundary LC molecules can greatly affect the light leakage in the dark state. Figures 10(a) and 10(b) show the two different rubbing diagrams in a VA and a MTN cell, respectively. Theoretically, rubbing diagram 2 accumulates less overall phase retardation than does rubbing diagram 1. This effect will be clearly demonstrated and further interpreted in the numerical simulations.

In calculating the contrast ratio, in order to approximate the guiding function and surface roughness of the micro-slant bumpy reflector, we simply let  $\theta_{\text{exit}}$  be scanned from  $0^\circ$  to  $20^\circ$  with a step of  $5^\circ$  at a fixed  $\theta_{\text{inc}} = -30^\circ$ . Figure 11 shows four viewing-angle-dependent contrast curves with different rubbing diagrams for both VA and  $80^\circ$  MTN cells. Here we take  $V = 0.7 V_{\text{rms}}$  and  $V = 5 V_{\text{rms}}$  as the OFF- and ON-state voltages for the VA cell. For the  $80^\circ$  MTN cell, the OFF- and ON-state voltages are defined at  $V = 5 V_{\text{rms}}$  and  $V = 0.7 V_{\text{rms}}$ , respectively. Under rubbing

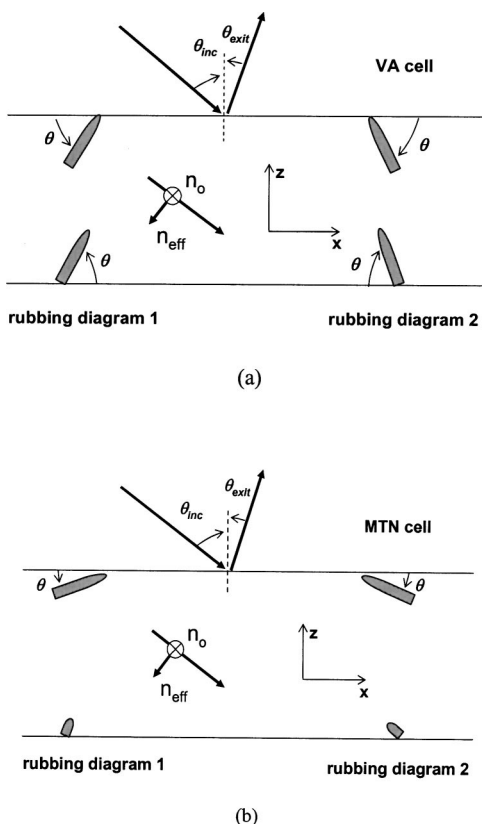


Fig. 10. Rubbing diagrams under asymmetric light incidence for (a) a VA cell, (b) a MTN cell.

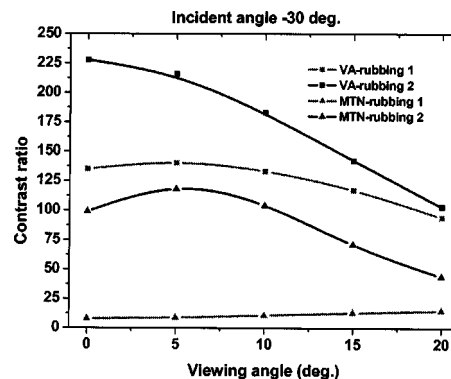


Fig. 11. Viewing-angle-dependent contrast-ratio plot for both VA and MTN modes under different rubbing diagrams.

diagram 1, the calculated contrast ratios for the VA cell at  $\theta_{\text{exit}} = 0^\circ, 5^\circ, 10^\circ, 15^\circ,$  and  $20^\circ$  are  $\sim 135:1, 140:1, 133:1, 116:1,$  and  $93:1$  at the above-mentioned OFF and ON states. The average contrast ratio is  $\sim 123:1$ . In the simulations, the internal multiple reflections by the indium-tin-oxide (ITO) layers are ignored, and we assume that in this small viewing cone the specular surface reflection is negligible owing to offset reflectance mechanism (no AR coating is used in the simulation). Otherwise, the simulated contrast ratio values may be reduced. If the VA cell is initialized under rubbing diagram 2, the corresponding contrast values are  $\sim 228:1, 216:1, 183:1, 142:1,$  and  $103:1$  with an average value of  $\sim 174:1$ . Sugiura *et al.*<sup>27</sup> reported a contrast value of  $\sim 80:1$  for a reflective VA mode with a slant reflector. The lower contrast ratio observed by Sugiura might originate from the imperfect elimination of a small amount of surface slant reflection and internal multiple reflections induced by the ITO electrodes, which degrade the contrast ratio. The rubbing-direction-induced contrast ratio difference for the VA cell here is not large because the nontwisted LC directors have large polar angles.

However, it can be seen from Fig. 11 that the rubbing diagram has a significant effect on the contrast ratio of an  $80^\circ$  MTN cell. The simulated contrast ratios at  $\theta_{\text{exit}} = 0^\circ, 5^\circ, 10^\circ, 15^\circ,$  and  $20^\circ$  are  $\sim 8:1, 9:1, 11:1, 13:1,$  and  $15:1$  with an average value of  $\sim 11:1$  under rubbing diagram 1. Once the cell is changed to the rubbing diagram 2, the corresponding contrast values are enhanced to  $\sim 99:1, 118:1, 104:1, 71:1,$  and  $44:1$  with an average value of  $\sim 87:1$ . The rubbing-diagram-induced contrast ratio difference is dramatic. In a high-voltage region (dark region), the central LC molecules tilt up almost perpendicularly to the substrate. But owing to the strong anchoring energy on the top boundary, the polar angle of the LC molecules will gradually decrease to the pretilt angle value ( $2^\circ$ ) with twist as their positions change from the center to the top of the cell. With this LC director profile in the dark state, the effective  $n_e$  values for the exit lights in the two diagrams are close to each other if the exit angle is close to the normal direction; i.e., the accumulated phase retardation for the reflected beams is little different between rubbing diagrams 1 and 2. However, for the incident beams (approximately  $-30^\circ$ ), the accumulated phase

retardation will have a much smaller value under rubbing diagram 2 than under rubbing diagram 1, since the parallel part of incident wave views a smaller effective  $n_e$  value under rubbing diagram 2. As a result, rubbing diagram 2 will produce much less overall residual phase retardation, which generates a higher contrast ratio. This phenomenon is not obvious in normal incidence. And the larger the difference between incident and exit angles, the more significant this effect will be in a MTN cell.

An ERSO group demonstrated a reflective LCD using 80° MTN cell and slant reflector.<sup>26</sup> For the case with  $\theta_{\text{inc}} = -30^\circ$  fixed and  $\theta_{\text{exit}}$  scanned from 0° to 20°, the experimentally measured maximum contrast ratio is >30:1. This result is somewhat lower than our simulated results. The imperfect elimination of a small amount of surface slant reflection and internal multiple reflections induced by the ITO electrodes are responsible for the degraded contrast ratio. Furthermore, in the ERSO experiments, it is observed that when the spot light source is fixed at  $\theta_{\text{inc}} = -30^\circ$ , the observed residual surface reflection always increases as the exit angle approaches from 0° to +20°. Here, if the small amount of surface reflection is the only dominant factor to determine the contrast ratio at small exit angles, it would predict a continuous decrease in contrast values as the exit angle gets larger, since the increasing surface specular reflections will degrade the contrast ratio dramatically. However, both the ERSO experiments and our numerical simulations show the contrast values first increase to a peak at  $\theta_{\text{exit}} = \sim 5^\circ$  and then decrease as the exit angle further increases. This phenomenon demonstrates that the light leakage from an LC cell is the dominant factor determining the contrast values, and our  $2 \times 2$  method is capable of obtaining the right modulation information of light from the LC cell under the asymmetric case.

To improve the contrast ratio of the normally white MTN display, the 90° twisted angle can be considered. In the voltage-on state, the phase retardations of the boundary layers compensate each other. As a result, the dark-state voltage is reduced and the contrast ratio is enhanced. A drawback of the 90° MTN cell, in comparison with the 80° MTN cell, is the slightly reduced reflectance.<sup>1,13</sup>

#### 4. CONCLUSIONS

We have derived two  $2 \times 2$  matrix representations: the unfolding method and the backward-eigenwave method for describing the asymmetric incident and exit angles of a realistic direct-view reflective LCD. In those symmetric cases, the  $2 \times 2$  matrix methods agree well with the  $4 \times 4$  matrix method, but their calculation speed is much faster than the  $4 \times 4$  matrix method. These two  $2 \times 2$  matrix methods are also applied to simulation of the normally black vertical alignment and the normally white mixed-mode twisted nematic reflective LCDs in a study of the contrast values of the asymmetric cases. A rubbing effect in the case of asymmetric incident and exit light is observed and analyzed. The simulated results agree reasonably well with the reported experimental data.

#### APPENDIX A: UNFOLDING METHOD

In a homogeneous-uniaxial-medium layer with tilt angle  $\theta$  and azimuthal angle  $\phi$ , we can express the dielectric tensor as<sup>17</sup>

$$\vec{\epsilon} = \begin{bmatrix} \epsilon_{xx} & \epsilon_{xy} & \epsilon_{xz} \\ \epsilon_{yx} & \epsilon_{yy} & \epsilon_{yz} \\ \epsilon_{zx} & \epsilon_{zy} & \epsilon_{zz} \end{bmatrix}, \quad (\text{A1})$$

with

$$\epsilon_{xx} = n_o^2 + (n_e^2 - n_o^2)\cos^2 \theta \cos^2 \phi, \quad (\text{A2a})$$

$$\epsilon_{xy} = \epsilon_{yx} = (n_e^2 - n_o^2)\cos^2 \theta \sin \phi \cos \phi, \quad (\text{A2b})$$

$$\epsilon_{xz} = \epsilon_{zx} = (n_e^2 - n_o^2)\sin \theta \cos \theta \cos \phi, \quad (\text{A2c})$$

$$\epsilon_{yy} = n_o^2 + (n_e^2 - n_o^2)\cos^2 \theta \sin^2 \phi, \quad (\text{A2d})$$

$$\epsilon_{yz} = \epsilon_{zy} = (n_e^2 - n_o^2)\sin \theta \cos \theta \sin \phi, \quad (\text{A2e})$$

$$\epsilon_{zz} = n_o^2 + (n_e^2 - n_o^2)\sin^2 \theta, \quad (\text{A2f})$$

where  $n_o$  and  $n_e$  are the ordinary and the extraordinary refractive index, respectively, of each medium layer. For absorption materials such as a polarizer, the refractive indices are complex values. With the dielectric-tensor information, the element extended Jones matrix for each layer can be specified.

For the  $i$ th sublayer, its element matrix  $J_i$  is equal to<sup>17</sup>

$$J_i = (SGS^{-1})_i, \quad (i = 1, 2, \dots, N), \quad (\text{A3})$$

with

$$S = \begin{bmatrix} 1 & c_2 \\ c_1 & 1 \end{bmatrix}, \quad (\text{A4})$$

$$G = \begin{bmatrix} \exp(ik_{z1}d_i) & 0 \\ 0 & \exp(ik_{z2}d_i) \end{bmatrix}, \quad (\text{A5})$$

where  $d_i$  is the thickness of the corresponding  $i$ th layer and

$$\frac{k_{z1}}{k_0} = \{[n_o^2 - (k_x/k_0)^2]\}^{1/2}, \quad (\text{A6})$$

$$\frac{k_{z2}}{k_0} = -\frac{\epsilon_{xz}k_x}{\epsilon_{zz}k_0} + \frac{n_o n_e}{\epsilon_{zz}} \left\{ \left[ \epsilon_{zz} - \left( 1 - \frac{n_e^2 - n_o^2}{n_e^2} \cos^2 \theta \sin^2 \phi \right) (k_x/k_0)^2 \right] \right\}^{1/2}, \quad (\text{A7})$$

$$c_1 = \frac{[(k_x/k_0)^2 - \epsilon_{zz}]\epsilon_{yx} + [(k_x/k_0)(k_{z1}/k_0) + \epsilon_{zx}]\epsilon_{yz}}{[(k_x/k_0)^2 + (k_{z1}/k_0)^2 - \epsilon_{yy}][\epsilon_{zz} - \epsilon_{yx} - \epsilon_{yz}\epsilon_{zy}]}, \quad (\text{A8})$$

$$c_2 = \frac{[(k_x/k_0)^2 - \epsilon_{zz}]\epsilon_{xy} + [(k_x/k_0)(k_{z2}/k_0) + \epsilon_{xz}]\epsilon_{zy}}{[(k_{z2}/k_0)^2 - \epsilon_{xx}][\epsilon_{zz} - \epsilon_{xy}] - [(k_x/k_0)(k_{z2}/k_0) + \epsilon_{zx}][\epsilon_{zz} - \epsilon_{xy} + \epsilon_{xz}]}.$$

Here  $k_x = k_0 \sin \theta$  is the  $x$  component of the wave vector, which is consistent in all layers, where  $k_0 = 2\pi/\lambda$  and  $\theta$  is the incident angle in air with respect to the  $+z$  axis.

## APPENDIX B: BACKWARD-EIGENWAVE METHOD

A complete solution of Maxwell's equation leads to the  $2 \times 2$  matrix formulations for the forward and backward waves. The procedures are similar to the  $4 \times 4$  matrix formulation, which can be derived by solving the eigenvalues and eigenvectors of the matrix denoting the linear Maxwell equations for transverse field components.<sup>9</sup>

In our derivation for the reflective LCDs with the backward-eigenwave method, we will take the coordinate system shown in Fig. 2. For simplicity, we normalize the magnetic field  $\mathbf{H}$  as

$$\hat{\mathbf{H}} = (\mu_0/\epsilon_0)^{1/2} \mathbf{H}. \quad (\text{B1})$$

Maxwell's equation can be expressed for  $\mathbf{E}$  and  $\hat{\mathbf{H}}$  in the following forms:

$$\nabla \times \mathbf{E} = ik_0 \hat{\mathbf{H}}, \quad (\text{B2a})$$

$$\nabla \times \hat{\mathbf{H}} = -ik_0 \vec{\epsilon} \mathbf{E}. \quad (\text{B2b})$$

With  $\partial/\partial y = 0$  and  $\partial/\partial x = ik_x$ , we can expand Eqs. (B2a) and (B2b) to six equations as

$$-\frac{\partial E_y}{\partial z} = ik_0 \hat{H}_x, \quad (\text{B3a})$$

$$-ik_x E_z + \frac{\partial E_x}{\partial z} = ik_0 \hat{H}_y, \quad (\text{B3b})$$

$$ik_x E_y = ik_0 \hat{H}_z, \quad (\text{B3c})$$

$$-\frac{\partial \hat{H}_y}{\partial z} = -ik_0 (\epsilon_{xx} E_x + \epsilon_{xy} E_y + \epsilon_{xz} E_z), \quad (\text{B3d})$$

$$-ik_x \hat{H}_z + \frac{\partial \hat{H}_x}{\partial z} = -ik_0 (\epsilon_{yx} E_x + \epsilon_{yy} E_y + \epsilon_{yz} E_z), \quad (\text{B3e})$$

$$ik_x \hat{H}_y = -ik_0 (\epsilon_{zx} E_x + \epsilon_{zy} E_y + \epsilon_{zz} E_z). \quad (\text{B3f})$$

After elimination of the longitudinal components, these six equations can be written in a matrix representation as

$$\frac{\partial}{\partial z} \begin{bmatrix} E_x \\ E_y \\ \hat{H}_x \\ \hat{H}_y \end{bmatrix} = ik_0 \mathbf{Q} \begin{bmatrix} E_x \\ E_y \\ \hat{H}_x \\ \hat{H}_y \end{bmatrix}, \quad (\text{B4})$$

where

$$\mathbf{Q} = \begin{bmatrix} -\frac{\epsilon_{zx}}{\epsilon_{zz}} \sin \theta_k & -\frac{\epsilon_{zy}}{\epsilon_{zz}} \sin \theta_k & 0 & 1 - \frac{\sin^2 \theta_k}{\epsilon_{zz}} \\ 0 & 0 & -1 & 0 \\ -\epsilon_{yx} + \epsilon_{yz} \frac{\epsilon_{zx}}{\epsilon_{zz}} & -\epsilon_{yy} + \epsilon_{yz} \frac{\epsilon_{zy}}{\epsilon_{zz}} + \sin^2 \theta_k & 0 & \frac{\epsilon_{yz}}{\epsilon_{zz}} \sin \theta_k \\ \epsilon_{xx} - \epsilon_{xz} \frac{\epsilon_{zx}}{\epsilon_{zz}} & \epsilon_{xy} - \epsilon_{xz} \frac{\epsilon_{zy}}{\epsilon_{zz}} & 0 & -\frac{\epsilon_{xz}}{\epsilon_{zz}} \sin \theta_k \end{bmatrix}. \quad (\text{B5})$$

From the theory of linear algebra, diagonalizing the  $\mathbf{Q}$  matrix to get its eigenvalues and eigenvectors can solve these coupled equations. This eigensystem can be solved by many numerical software programs. By this method, we can express the diagonalized  $\mathbf{Q}$  matrix as

$$\mathbf{Q} = \mathbf{T} \begin{bmatrix} q_1 & & & \\ & q_2 & & \\ & & q_3 & \\ & & & q_4 \end{bmatrix} \mathbf{T}^{-1}, \quad (\text{B6})$$

where  $q_1$  to  $q_4$  are the eigenvalues of  $\mathbf{Q}$ , and  $\mathbf{T}$  is composed of the corresponding eigenvectors. For simplicity,

we intentionally adjust the  $q$  eigenvalues and the eigenvector matrix  $\mathbf{T}$  in a way such that  $q_1$  and  $q_2$  are positive and  $q_3, q_4$  are negative.

With the diagonalized  $\mathbf{Q}$  matrix, we can further conduct a variable transformation of the tangential field components as

$$\begin{bmatrix} E_x \\ E_y \\ \hat{H}_x \\ \hat{H}_y \end{bmatrix} = \mathbf{T} \begin{bmatrix} U_1 \\ U_2 \\ U_3 \\ U_4 \end{bmatrix}, \quad (\text{B7})$$

where  $\mathbf{T}$  is expanded as

$$\mathbf{T} = \begin{bmatrix} \mathbf{T}_{11} & \mathbf{T}_{12} \\ \mathbf{T}_{21} & \mathbf{T}_{22} \end{bmatrix}. \quad (\text{B8})$$

Substituting Eq. (B7) into Eq. (B4), we can obtain

$$\frac{\partial}{\partial z} \begin{bmatrix} U_1 \\ U_2 \\ U_3 \\ U_4 \end{bmatrix} = ik_0 \begin{bmatrix} q_1 & & & \\ & q_2 & & \\ & & q_3 & \\ & & & q_4 \end{bmatrix} \begin{bmatrix} U_1 \\ U_2 \\ U_3 \\ U_4 \end{bmatrix}. \quad (\text{B9})$$

Equation (B9) comprises four uncoupled equations in which  $U_1$  and  $U_2$  represent the forward eigenwaves and  $U_3$  and  $U_4$  represent the backward ones. According to Fig. 12, the solutions of Eq. (B9) are

$$\begin{bmatrix} U_1 \\ U_2 \\ U_3 \\ U_4 \end{bmatrix}_{n,d_n} = \mathbf{G}_n \begin{bmatrix} U_1 \\ U_2 \\ U_3 \\ U_4 \end{bmatrix}_{n,0}, \quad (\text{B10})$$

where

$$\mathbf{G}_n = \begin{bmatrix} \exp(ik_{z1}d_n) & & & \\ & \exp(ik_{z2}d_n) & & \\ & & \exp(ik_{z3}d_n) & \\ & & & \exp(ik_{z4}d_n) \end{bmatrix}, \quad (\text{B11})$$

and

$$k_{z1} = k_0q_1, \quad (\text{B12a})$$

$$k_{z2} = k_0q_2, \quad (\text{B12b})$$

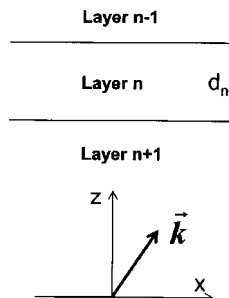


Fig. 12. Structure of  $n$ th sublayer with thickness  $d_n$ . Notice that the bottom of this layer is the  $(n+1)$ st layer.

$$k_{z3} = k_0q_3, \quad (\text{B12c})$$

$$k_{z4} = k_0q_4. \quad (\text{B12d})$$

For the forward eigenwaves, we can correlate the  $U_1$  and  $U_2$  values on the top and bottom surfaces of the  $n$ th layer as

$$\begin{bmatrix} U_1 \\ U_2 \end{bmatrix}_{n,d_n} = \mathbf{F}_n \begin{bmatrix} U_1 \\ U_2 \end{bmatrix}_{n,0}, \quad (\text{B13})$$

where

$$\mathbf{F}_n = \begin{bmatrix} \exp(ik_{z1}d_n) & 0 \\ 0 & \exp(ik_{z2}d_n) \end{bmatrix}. \quad (\text{B14})$$

A similar relation for the backward parts  $U_3$  and  $U_4$  can be expressed as

$$\begin{bmatrix} U_3 \\ U_4 \end{bmatrix}_{n,d_n} = \mathbf{B}_n \begin{bmatrix} U_3 \\ U_4 \end{bmatrix}_{n,0}, \quad (\text{B15})$$

with

$$\mathbf{B}_n = \begin{bmatrix} \exp(ik_{z3}d_n) & 0 \\ 0 & \exp(ik_{z4}d_n) \end{bmatrix}. \quad (\text{B16})$$

From Eqs. (B7) and (B8), the corresponding electric fields can be expressed by the forward (+) and backward (-) eigenwaves as

$$\begin{bmatrix} E_x \\ E_y \end{bmatrix} = \begin{bmatrix} E_x \\ E_y \end{bmatrix}^+ + \begin{bmatrix} E_x \\ E_y \end{bmatrix}^- = \mathbf{T}_{11} \begin{bmatrix} U_1 \\ U_2 \end{bmatrix} + \mathbf{T}_{12} \begin{bmatrix} U_3 \\ U_4 \end{bmatrix}. \quad (\text{B17})$$

According to the fact that in conventional LCDs the backward eigenwaves are negligible, from Eq. (B17) we obtain the further expression:

$$\begin{bmatrix} E_x \\ E_y \end{bmatrix} \approx \begin{bmatrix} E_x \\ E_y \end{bmatrix}^+ = \mathbf{T}_{11} \begin{bmatrix} U_1 \\ U_2 \end{bmatrix}. \quad (\text{B18})$$

Because the  $x$  and  $y$  field components are continuous on the interference of a layer, from Eqs. (B13) and (B18) and Fig. 12, electric fields between subsequent layers can be correlated as

$$\begin{bmatrix} E_x \\ E_y \end{bmatrix}_n^+ = \mathbf{J}_{e,n}^+ \begin{bmatrix} E_x \\ E_y \end{bmatrix}_{n+1}^+, \quad (\text{B19})$$

where

$$\mathbf{J}_{e,n}^+ = (\mathbf{T}_{11})_n \mathbf{F}_n (\mathbf{T}_{11})_n^{-1} \quad (\text{B20})$$

is the transforming matrix for forward tangential-field components of subsequent layers. Here the layer index is defined in the same way as shown in Fig. 2. For the negligible backward field components, a similar relation can be given as

$$\begin{bmatrix} E_x \\ E_y \end{bmatrix}^- = \mathbf{T}_{12} \begin{bmatrix} U_3 \\ U_4 \end{bmatrix}. \quad (\text{B21})$$

Along with Eq. (B15) and Fig. 12, we can express the backward tangential-field components between subsequent layers by

$$\begin{bmatrix} E_x \\ E_y \end{bmatrix}_{n+1}^- = (\mathbf{J}_{e,n}^-)^{-1} \begin{bmatrix} E_x \\ E_y \end{bmatrix}_n^-, \quad (\text{B22})$$

where

$$(\mathbf{J}_{e,n}^-)^{-1} = (\mathbf{T}_{12})_n (\mathbf{B}_n)^{-1} (\mathbf{T}_{12})_n^{-1} \quad (\text{B23})$$

is the transforming matrix. Here we intentionally express the backward tangential components at layer  $n+1$  by those at layer  $n$  to denote the incident wave in reflective LCDs.

## ACKNOWLEDGMENTS

We are indebted to Toppoly Optoelectronics Corporation (Taiwan) for financial support.

Corresponding author Shin-Tson Wu's e-mail address is swu@mail.ucf.edu.

## REFERENCES

1. S. T. Wu and D. K. Yang, *Reflective Liquid Crystal Displays* (Wiley, New York, 2001).
2. M. F. Schiekel and K. Fahrenschon, "Deformation of nematic liquid crystals with vertical orientation in electrical fields," *Appl. Phys. Lett.* **19**, 391–393 (1971).
3. S. T. Wu and C. S. Wu, "Mixed-mode twisted nematic liquid crystal cells for reflective displays," *Appl. Phys. Lett.* **68**, 1455–1457 (1996).
4. S. Teitler and B. W. Hennis, "Refraction in stratified, anisotropic media," *J. Opt. Soc. Am.* **60**, 830–834 (1970).
5. D. W. Berreman, "Optics in stratified and anisotropic media:  $4 \times 4$  matrix formulation," *J. Opt. Soc. Am.* **62**, 502–510 (1972).
6. I. Abdulhalim, L. Benguigui, and R. Weil, "Selective reflection by helicoidal liquid crystals. Results of an exact calculation using the  $4 \times 4$  characteristic matrix method," *J. Phys. Colloq.* **46**, 815–825 (1985).
7. I. Abdulhalim, R. Weil, and L. Benguigui, "Dispersion and attenuation of the eigenwaves for light propagation in helicoidal liquid crystals," *Liq. Cryst.* **1**, 155–167 (1986).
8. H. Wohler, G. Hass, M. Fritsch, and D. A. Mlynski, "Faster  $4 \times 4$  matrix method for uniaxial inhomogeneous media," *J. Opt. Soc. Am. A* **5**, 1554–1557 (1988).
9. K. Eidner, G. Mayer, M. Schmidt, and H. Schmiedel, "Optics in stratified media—the use of optical eigenmodes of uniaxial crystal in the  $4 \times 4$  matrix formalism," *Mol. Cryst. Liq. Cryst.* **172**, 191–200 (1989).
10. C. J. Chen, A. Lien, and M. I. Nathan, " $4 \times 4$  and  $2 \times 2$  matrix formulations for the optics in stratified and biaxial media," *J. Opt. Soc. Am. A* **14**, 3125–3133 (1997).
11. I. Abdulhalim, "Analytic propagation matrix method for linear optics of arbitrary biaxial layered media," *J. Opt. A, Pure Appl. Opt.* **1**, 646–653 (1999).
12. S. Stallinga, "Berreman  $4 \times 4$  matrix method for reflective liquid crystal displays," *J. Appl. Phys.* **85**, 3023–3031 (1999).
13. C. L. Kuo, C. K. Wei, S. T. Wu, and C. S. Wu, "Reflective direct-view display using a mixed-mode twisted nematic cell," *Jpn. J. Appl. Phys., Part 1* **36**, 1077–1080 (1997).
14. P. G. De Gennes and J. Prost, *The Physics of Liquid Crystals*, 2nd ed. (Oxford, London, 1995).
15. P. Yeh, "Extended Jones matrix method," *J. Opt. Soc. Am.* **72**, 507–513 (1982).
16. C. Gu and P. Yeh, "Extended Jones matrix method II," *J. Opt. Soc. Am. A* **10**, 966–973 (1993).
17. A. Lien, "Extended Jones matrix representation for the twisted nematic liquid-crystal display at oblique incidence," *Appl. Phys. Lett.* **57**, 2767–2769 (1990).
18. A. Lien and C. J. Chen, "A new  $2 \times 2$  matrix representation for twisted nematic liquid crystal displays at oblique incidence," *Jpn. J. Appl. Phys., Part 1* **35**, L1200–L203 (1996).
19. A. Lien, "A detailed derivation of extended Jones matrix representation for twisted nematic liquid crystal displays," *Liq. Cryst.* **22**, 171–175 (1997).
20. F. H. Yu and H. S. Kwok, "Comparison of extended Jones matrices for twisted nematic liquid-crystal displays at oblique angles of incidence," *J. Opt. Soc. Am. A* **16**, 2772–2780 (1999).
21. I. Abdulhalim, "Exact  $2 \times 2$  matrix method for the transmission and reflection at the interface between two arbitrarily oriented biaxial crystals," *J. Opt. A, Pure Appl. Opt.* **1**, 655–661 (1999).
22. I. Abdulhalim, " $2 \times 2$  Matrix summation method for multiple reflections and transmissions in a biaxial slab between two anisotropic media," *Opt. Commun.* **163**, 9–14 (1999).
23. M. Mansuripur, "Analysis of multilayer thin-film structures containing magneto-optic and anisotropic media at oblique incidence using  $2 \times 2$  matrices," *J. Appl. Phys.* **67**, 6466–6475 (1990).
24. E. Cojocar, "Generalized Abel's relations for an anisotropic thin film of an arbitrary dielectric tensor," *Appl. Opt.* **36**, 2825–2829 (1997).
25. S. Pancharatnam, "Achromatic combination of birefringent plates. II. An achromatic quarter-wave plate," *Proc. Indian Acad. Sci., Sect. A* **41**, 137–144 (1955).
26. D. L. Ting, W. C. Chang, C. Y. Liu, J. W. Shiu, C. J. Wen, C. H. Chao, L. S. Chuang, and C. C. Chang, "A high brightness and high contrast reflective LCD with micro slant reflector (MSR)," *SID Int. Symp. Digest Tech. Papers* **30**, 954–957 (1999).
27. N. Sugiura, K. Tashiro, K. Ohmuro, Y. Koike, and K. Okamoto, "A novel vertically aligned reflective-color TFT LCD with high contrast ratio," *SID Int. Symp. Digest Tech. Papers* **33**, 1386–1389 (2002).